Received: 2 September 2020 | Revised: 25 November 2020 | Accepted: 26 November 2020

DOI: 10.1002/pen.25610

RESEARCH ARTICLE

POLYMER ENGINEERING AND SCIENCE WILEY

Electrical insulation properties of silicone rubber under accelerated corona and thermal aging

El Hadi Belhiteche[1,2] | **Sébastien Rondot**[3] | **Mustapha Moudoud**[1,4] | **Philippe Dony**[3] | **Omar Jbara**[3]

[1]Laboratoire des Technologies Avancées en Génie Electrique (LATAGE), Université de Tizi-Ouzou, Tizi-Ouzou, Algeria

[2]Université Mohamed Boudiaf, M'Sila, Algeria

[3]Institut de Thermique, Mécanique et Matériaux–Université de Reims, UFR Sciences, Université de Reims, Reims, France

[4]Département d'Electrotechnique, Université Mouloud Mammeri, Tizi-Ouzou, Algeria

Correspondence
El Hadi Belhiteche, Laboratoire des Technologies Avancées en Génie Electrique (LATAGE), UMMTO, BP 17 RP 15000 Tizi-Ouzou, Algerie.
Email: [redacted]@univ-msila.dz

Funding information
Algerian Ministry of Higher Education and Scientific Research

Abstract

A contactless method based on energy shift of high-energy cut-off of the x-ray bremsstrahlung, the so-called Duane Hunt Limit and a conventional low voltage electrical technique (three-probes technique) is applied on thermal and corona aged silicone rubber (SiR) to measure, respectively, the surface potential, V_s, and the surface resistivity, ρ_s. The effect of aging on these quantities, representing the dielectric properties, is studied. The results are highly reproducible and highlight a good correlation between V_s and ρ_s. It was observed that thermal aging combined with electrical aging deteriorates more the electrical properties of the polymer than thermal aging alone. Explanations for electrical characteristics (V_s, ρ_s) change with aging are supported by attenuated total reflection Fourier transform infrared spectroscopy spectra analysis and a chemical mechanism of aging in three steps (i.e., oxidation-polycondensation, degradation, and thermal cracking). The surface degradation of the polymer is revealed by images of surface morphology obtained by using scanning electron microscopy (SEM). Roughness is greater for combined thermal and corona aging mode compared to thermal aging alone. In addition, the surface degradation of SiR polymer is confirmed by the loss of its hydrophobicity.

KEYWORDS

corona discharge, electrical properties, FTIR-ATR, silicone rubber, surface degradation, thermal aging

1 | INTRODUCTION

Polymers are employed in a widespread range of applications, such as power cables, film capacitors, overhead power line insulators, surge arresters, and so forth.[1,2] In these applications, the electrical properties of polymers are major aspects that need to be investigated prior to implementation. During their service, the polymers are subjected to various stresses in particular thermal and electrical ones.[3] Aging and resulting electrical insulation degradation are then unavoidable. In the long run, this may lead to costly failure.[4] Understanding the aging process is essential to achieve better quality materials that will provide an extended lifetime of the insulation. Since the assumed lifetime can reach several decades and it is impossible to make aging tests during this long time, the alternative often adopted is accelerated aging.[5] In this work, accelerated thermal aging and a combination of thermal and corona discharge aging have been achieved. These aging modes have been chosen because in most electrical applications, they reduce the reliability of a system by degrading insulation.[6,7] Moreover, the effects of corona are cumulative and permanent, and failure can occur without warning signs.[6] Many research

works have been developed on this subject.[8,9] Despite of the progress made up to now, results are still sometimes contradictory and difficult to reproduce. Any new insight into this problem is a step further in preventing failure of the insulation and increasing its useful lifetime.

The purpose of this contribution is to relate aging to changes in surface dielectric properties of silicone rubber (SiR) using different experimental techniques, such as energy dispersive X-ray spectrometry (EDS), conventional electrical technique, attenuated total reflection Fourier transform infrared spectroscopy (ATR-FTIR), and scanning electron microscopy (SEM). The choice of measurement techniques of surface potential V_s and surface resistivity ρ_s, is justified by aging, which affects primarily the surface of sample. These techniques give complementary information. Measurement of surface resistivity is a macroscopic parameter that concerns the entire surface of samples while Vs measurement concerns the analysis of the degradation processes that takes place in a relatively small local area (ten square millimeters) at the surface. They allow the homogeneity of sample and effect of aging to be checked. The hydrophobicity was also evaluated using the measurement of the contact angle of a drop of water with the polymer surface.[8] SEM images were used to highlight the surface degradation of the polymer for both aging modes. After presenting aging procedures and characterization methods in Section 2, the results obtained were analyzed. The trends obtained for the resistivity and the surface potential when the aging time increased were interpreted on the basis of the ATR-FTIR spectra supported by a chemical mechanism in three steps (i.e., oxidation-polycondensation, degradation, and thermal cracking). These results highlight a good correlation between V_s and ρ_s and show that thermal aging combined with the electrical aging deteriorates more the electrical properties of the polymer.

2 | EXPERIMENTAL

2.1 | Samples preparation and observation

Solid elastomer SiR material was manufactured and provided by the German company Wacker Chemie. It contains polymers with a high molecular weight, relatively long polymer chains, and 4 to 5% of alumina trihydrate (ATH). This material is referred to as high-temperature-vulcanizing polymer. In this study, samples of 25×25 mm^2 area and 6 mm thick were used. Two types of aging have been carried out, the thermal aging alone and the combination of thermal aging and electrical aging by corona discharge. In this last case, the thermal aging was made before the electrical one. The thermal aging of SiR samples was made at 190°C, in forced air-circulating oven that could maintain the average temperature of the samples with a precision of ±1°C. The temperature of 190°C is chosen based on the data available in the literature. Indeed, this temperature produces a measurable degradation of the material without high decomposition after in a reasonable time.[10–12]

The samples were vertically suspended in the oven in order to be in contact with the circulating air leading to a homogeneous aging. The time of thermal aging is ranging from 100 to 1200 h.

Corona discharge[13] was performed using the test arrangement shown in Figure 1. It consists of sphere-to-plane geometrical electrodes. The plane electrode is made in copper. The spherical steel electrode has a radius of 6 mm. The gap between the spherical electrode and the surface of sample was 3 mm. To avoid side effects, the edges of the plane electrode were rounded off. High voltage test transformer (100 kV, 10 kVA, 50 Hz) along with a control panel was used for applying electrical stresses. The geometrical configuration of sphere-to-plane electrodes can be used for positive or negative corona discharge. For more details, a comparative study of the corona discharge with electrodes of different geometries may be consulted.[14] The sample (SiR polymer) was placed on the flat electrode connected to the ground. The upper surface of the sample was opened to the surrounding air. The aging was carried out using positive corona discharge during 8 h with a voltage of 12 kV applied between electrodes. The electrical field in the air gap was approximately 4 kV/mm.

The topography of the samples was observed using environmental scanning electron microscope (ESEM) FEI/Philips XL30 with an accelerating voltage of 20 kV. Secondary electron images are acquired on pristine and aged samples. The scanned area was 1000 μm^2.

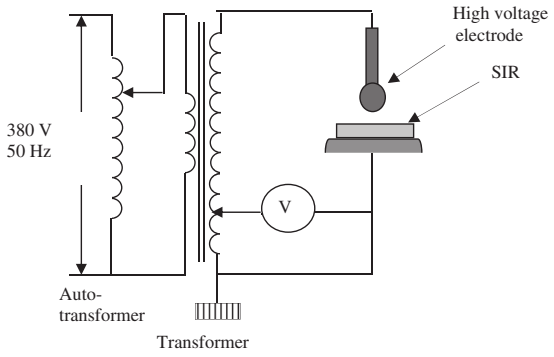

FIGURE 1 Schematic diagram of the experimental setup used for corona discharge

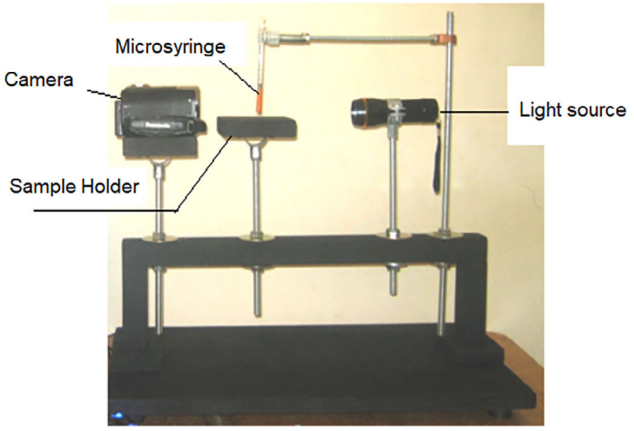

FIGURE 2 Experimental setup for hydrophobicity measurements [Color figure can be viewed at wileyonlinelibrary.com]

2.2 | Hydrophobicity measurement

In this paper, the detection of the degree of hydrophobicity, that is, the state of CH3 group is obtained by measuring the static contact angle. The degree of hydrophobicity of the insulating material gives an idea of the aging state of the insulator.[15] Indeed, the hydrophobicity depends on the roughness of the surface and the chemical composition. Changes in these parameters can adjust the values of the contact angle and, therefore, the hydrophobicity. The surface changes (e.g., morphology and chemistry) also affects the density and mobility of charge carriers, hence the surface potential and the surface resistivity. Polymer surface can easily be modified by corona discharges or thermal aging. This modification leads to the oxidation of the surface and the creation of new chemical groups containing mainly oxygen. Immediately after aging, the values of the contact angles of the polymer decrease considerably.[16] These processes increased the density and mobility of the charge carriers leading to an increase of conductivity and, therefore, to a decrease of V_s and ρ_s.[17] The surface hydrophobicity of SiR polymer was measured in terms of its contact angle. A drop of deionized water with volume between 4 and 5 μL, was deposited using a micro syringe on previously cleaned surface of this polymer. To determinate the contact angle characterizing the hydrophobicity, a photo of the drop was taken by a digital camera and treated using the AutoCAD software.[18] This procedure is equivalent to using a goniometer.[8] The photo in Figure 2 shows the implemented experimental set up. The data of the contact angle were obtained from the mean of six to nine measurements that were made on different drops placed on the surface.

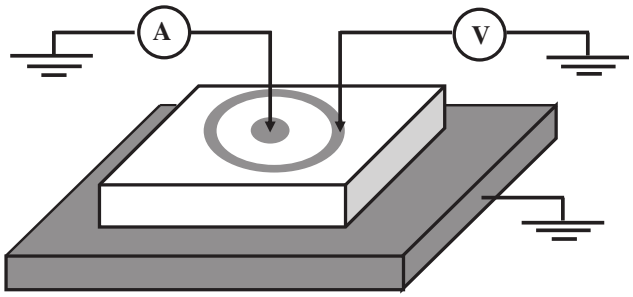

FIGURE 3 Experimental setup for surface resistivity measurement

2.3 | Surface resistivity

The determination of electrical surface resistivity of the sample has been performed by measuring its electrical surface resistance when placed in a setup composed of three metallic electrodes. The electrode system that was used to perform the measurements was made up according to the recommendations of ASTM D-257 standard test method for DC resistance.[19,20] The geometry of this electrode system allowed the relation between electrical resistance and resistivity to be easily determined. A schematic diagram of the experimental setup is shown in Figure 3. A HP4140B picoammeter/DC voltage source was used to apply a DC voltage ramp between the concentric electrodes.

The surface resistance R_s, deduced from obtained current–voltage curve, was then analyzed to determine the resistivity, ρ_s, following[21]:

$$\rho_s = 2\pi.Rs.\ln(D2/D1) \quad (1)$$

where D_2 and D_1 are, respectively, the inner diameter of the external electrode and the central electrode diameter.

2.4 | Surface potential from EDS spectrometry in SEM

EDS spectra were obtained using a SEM Jeol 6460LA LVSEM equipped with an EDS system. Experimental conditions, such as high-vacuum mode 10^{-5} torr, electron beam energy 15 keV, working distance 10 mm, scan size, and scan rate was kept constant during acquisition of EDS X-ray data. To obtain satisfactory X-ray signal-to-noise ratios (i.e., counting rate > 3000 cps.), the electron beam current (2 nA) and X-ray spectrum acquisition time (300 live seconds per spectrum) were chosen and kept constant. The experimental arrangement used for this part is given in Figure 4.

In this study, the surface potential was due to negative charging induced under the electronic irradiation of

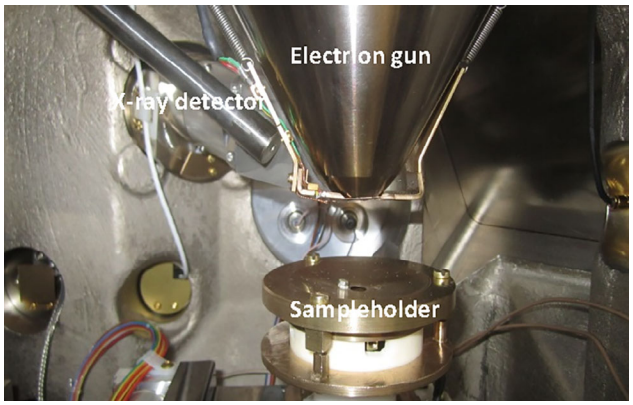

FIGURE 4 Schematic illustration of the experimental arrangement used for the surface potential measurements in insulators [Color figure can be viewed at wileyonlinelibrary.com]

the sample in (SEM) as illustrated by Figure 4. When a highly resistive sample is submitted to an electron irradiation, the negative charging causes strong charging effects often undesirable during imaging in the SEM or in Auger electron spectroscopy. However, these effects can be used to conveniently monitor the surface potential. There are several techniques to determine the surface potential under electron irradiation, such as the mirror method[22] and methods based on energy shifts in high-energy cutoff of the X-ray bremsstrahlung the so-called Duane–Hunt limit (DHL).[23] This last contactless method was used to determine the surface potential. The DHL represents the highest energy continuum X-ray that can be generated by an incident electron, thus it is equal to the energy of the primary electron itself. When the specimen acquires negative charge, the resulting field acts to decelerate the incoming beam electrons, lowering their impact kinetic energy relative to that with which they left the electron gun. This effect can be expressed most easily in terms of the surface potential V_s that develop. Indeed, primary electrons with kinetic energy E_0 begin slowing down before they encounter the surface such that they impact with a landing energy of $E_o - e|V_s|$. Thus, the surface potential at the steady state may be measured from the shift of the DHL. Typical X-ray EDS spectrum of silicon rubber acquired at the steady state for unaged sample and a 1200 h aging time is shown in Figure 5(A),B, respectively. As explained above, the surface potential at the steady state, deduced from the shift of the DHL in Figure 5(B) is $V_s = 7900$ V.

Compared to noncontact electrostatic voltmeter,[24] which is usually used, the DHL method has a good resolution and the measurement of V_s is carried out at the steady state during irradiation. In the first method V_s is measured after the irradiation of the specimen, which may have lost a part of its charge.

2.5 | ATR-FTIR analysis

IR-measurements were performed in ATR mode as the sample was too thick to be used in conventional transmission mode. The ATR mode is commonly used to probe surface properties of materials rather than their bulk properties. Measurements were performed with a spectrometer FTIR SHIMADZU-8400S type, with an ATR device (PIKE Technologies MIRacleZnSe/diamond) in the spectral range 4000–650 cm^{-1}. This set-up allowed to collect spectra with a spectral resolution of 4 cm^{-1} and to analyze the data using a dedicated software package. Each spectrum results from an averaging of 40 scans.

3 | RESULTS AND DISCUSSION

3.1 | Morphology of samples

Secondary electron images acquired using an ESEM technique are shown in Figure 6, on unaged and aged samples. The aging time was 1200 h. Aging has an effect on the topography of the polymer surface. The unaged samples have a relatively smooth surface, while the aged samples have their surface layer peeled off. This layer, consisting mainly of polymer, is gradually replaced during aging by a mixture of polymer and fillers.[8] This process has the effect of increasing the roughness of the surface of the sample as shown by images presented above. It was observed that the roughness is greater in the case of combined thermal and corona aging mode.

3.2 | Mechanism of chemical change of SiR

The thermal aging of the polymer in an oven under air atmosphere at 190°C leads to the modification over time of composition and morphology of the polymer surface. This is explained by the mechanism commonly invoked. It essentially involves three consecutive physico-chemical processes[5,9] namely thermal oxidation (1), polycondensation (2), thermal degradation, and cracking (3) (see Figure 7). In air, the side groups of the SiR were oxidized with oxygen (see reaction 1). Since the Si—O bond has both covalent and ionic characteristics, dissolution of the Si—O structure resulted in SiR degradation under high temperature conditions (see reaction 2). The reaction of the thermal crack leads to breaking of the molecular chain into small cyclic molecules (see reaction 3). Thermal crack reaction occurred at higher temperatures and longer aging times than thermal oxidation and thermal degradation reactions.

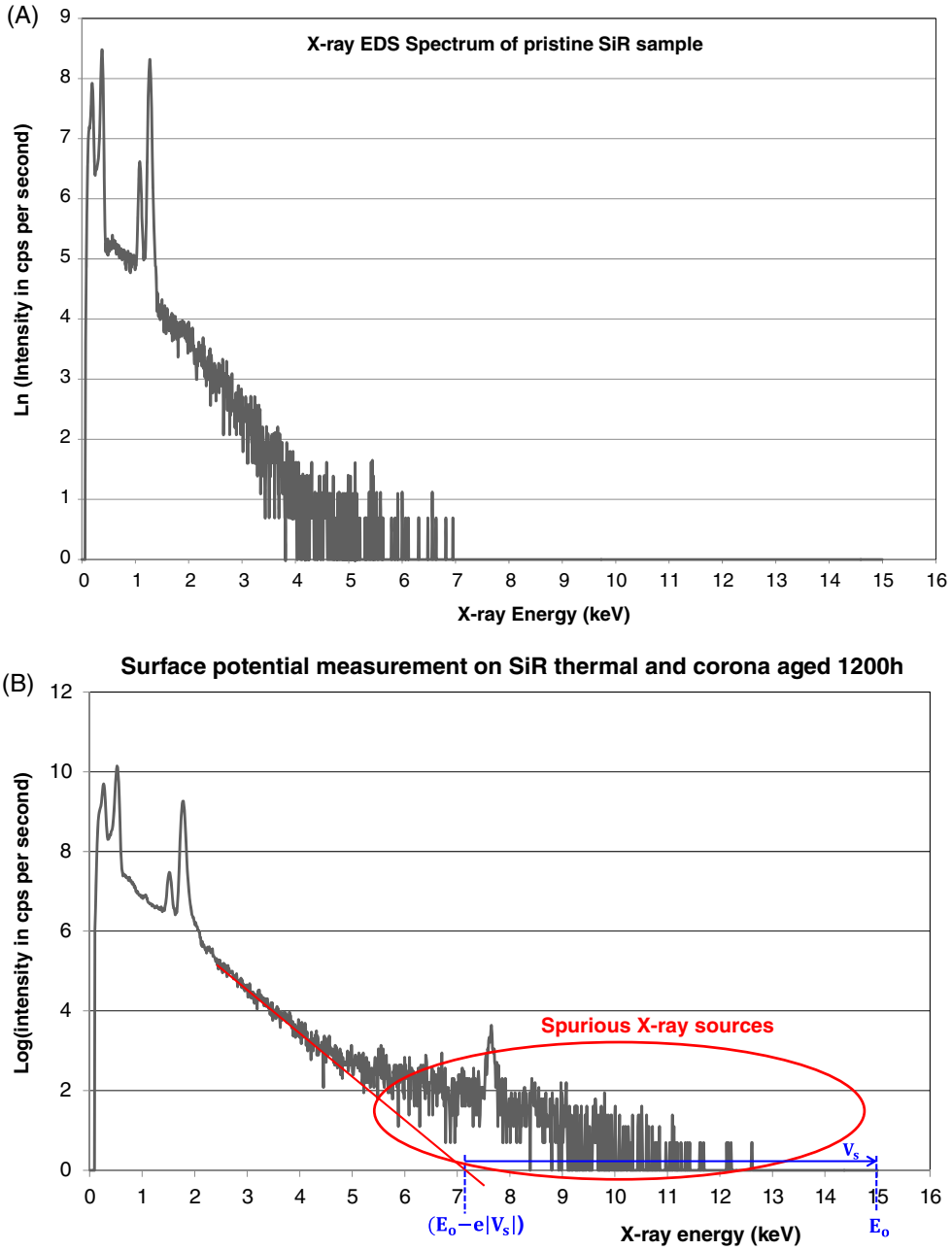

FIGURE 5 (A) X-ray spectrum of unaged SiR simple. (B) X-ray spectrum of SiR obtained at primary beam energy $E_0 = 15$ keV and primary beam current $I_0 = 1$ nA. The part of the spectrum bounded by the circle corresponds to the X-rays generated by the spurious electrons coming from the microscope chamber [Color figure can be viewed at wileyonlinelibrary.com]

3.3 | ATR-FTIR analysis

ATR-FTIR technique was used to identify the evolution of main chemical bonds during aging of SiR as depicted in Figure 8. As spectra corresponding to both types of aging (thermal and thermal + corona) are identical, we have presented only one spectrum (thermal aging one) in this figure. Corona treatment acts only on few nanometers depth of SiR samples by ionic erosion and UV irradiation whereas ATR-FTIR depth analysis is around few micrometers. This technique is then not sensitive to surface composition changes induced by corona discharge.

For FTIR identification, the wave numbers and their corresponding functional groups related to the studied material are deduced from references[25-27] and shown in Table 1. Relative intensities of each peak in Figure 8, normalized to the most intense peak (790 cm^{-1} Si $(CH_3)_2$ bond) at 1200 h are also given in Table 1.

The evolution of the normalized intensities of the different peaks during thermal aging is explained by their action mechanism seen before (Figure 7). The band 3800–3200 cm^{-1} corresponds to the OH groups linked by a hydrogen bond in ATH ($Al_2O_3 \cdot 3H_2O$) introduced in the polymer as filler (flame retardant) on one hand and water absorbed by the polymer on the other hand. It can be seen that its intensity decreased steadily up to 600 h except for a slight increase observed at 336 h. This

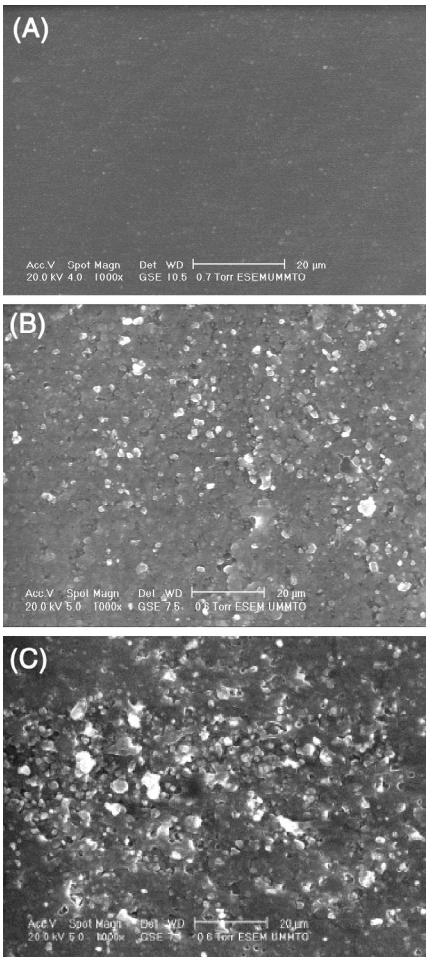

FIGURE 6 ESEM micrographs of SiR samples. (A) Unaged, (B) after thermal aged, and (C) after thermal and corona discharges aged. Aging time was 1200 h

intensity increased also until 960 h and then decreased sharply thereafter.

The initial decrease (up to 96 h) is related to the decomposition of the ATH, which loses its water by dehydration according to the following mechanism[28]:

$$Al2O3 \cdot 3H2O \overset{Heat}{\rightarrow} Al2O3 + 3H2O.$$

This band includes also the stretching mode of Si—OH bond, the intensity of which should increase owing to Si—OH groups formed following oxidation (reaction 1). This trend was not observed experimentally at the beginning (before 96 h) because it was probably masked by the vibration mode associated with the OH bond of water in ATH seen before (OH bonds of ATH are preponderant compared to those of Si—OH at the beginning of thermal aging). However, from 96 h after the evaporated ATH water, Si—OH bonds were evidenced by the increase of the peak 3440 cm^{-1} at 336 h (reaction 1). From 336 to 600 h there was a decrease in this peak related to the cross linking of the chains (reaction 1). This resulted in the formation of water supported by the increase of the peak at 1650 cm^{-1} corresponding to the OH group of the water of crystallization. After 600 h the formed water began to disappear and the Si—OH bonds are again predominant compared to OH groups leading to increase of the peak 3440 cm^{-1}. Indeed, the increase from 600 to 960 h was due to the formation of OH^- ions resulting from the Si—OH bonds breaking under the effect of heat and after a long aging time. This is the beginning of reaction 2 where these OH^- ions caused the breaking of Si—O—Si bonds and the appearance of siloxy ions $Si—(CH_3)_2—O^-$ that exerted major influence on the formation of oligomers and accelerated degradation process.[29,30] At 1200 h, the sharp decrease of the peak 3440 cm^{-1} is associated with the total disappearance of the OH— ions because of polymer cracking, leading to cyclic molecules (reaction 3).

The peak at 1650 cm^{-1} corresponds to OH bond of water of crystallization (i.e. hydration). Its low intensity for low aging times suddenly increased at 600 h and decreased beyond this time to cancel at 1200 h. Indeed, at the beginning of the degradation process (from 600 h), water formed in volume during the oxidation-polycondensation processes moved upwards to the surface (i.e., intensity increased) to desorbs thereafter (i.e., intensity decreased).

The peak intensity corresponding to the Si—C bond stretching at 790 $cm^{-1}$is assigned to the strong stretching vibration $Si—(CH3)_2$[31,32] group decreased first slightly, remained constant and then increased to around 1200 hours. The decrease was due to the partial disappearance of these bonds during oxidation and polycondensation (i.e., crosslinking), while the increase is associated with the cracking, giving cyclic molecules with a greater degree of freedom for the $Si—CH_3$ bonds.

The intensity of the Si—O—Si peak seemed to increase very slightly up to 600 h, presented a small plateau and then increased from 960 h. Indeed, the polycondensation was responsible for the creation of Si—O—Si bridges and from 600 h the polymer began to degrade giving smaller chains (breaking Si—O—Si bonds in the chain). The final increase is related to the formation of cyclic molecules.

3.4 | Hydrophobicity measurement

The hydrophobicity tests were conducted following the methodology described (see Section 2.2) and the standard classification STRI Guide ([8] and references therein). The results obtained for the two types of aging are gathered in

FIGURE 7 Chemical processes of SiR under thermal aging

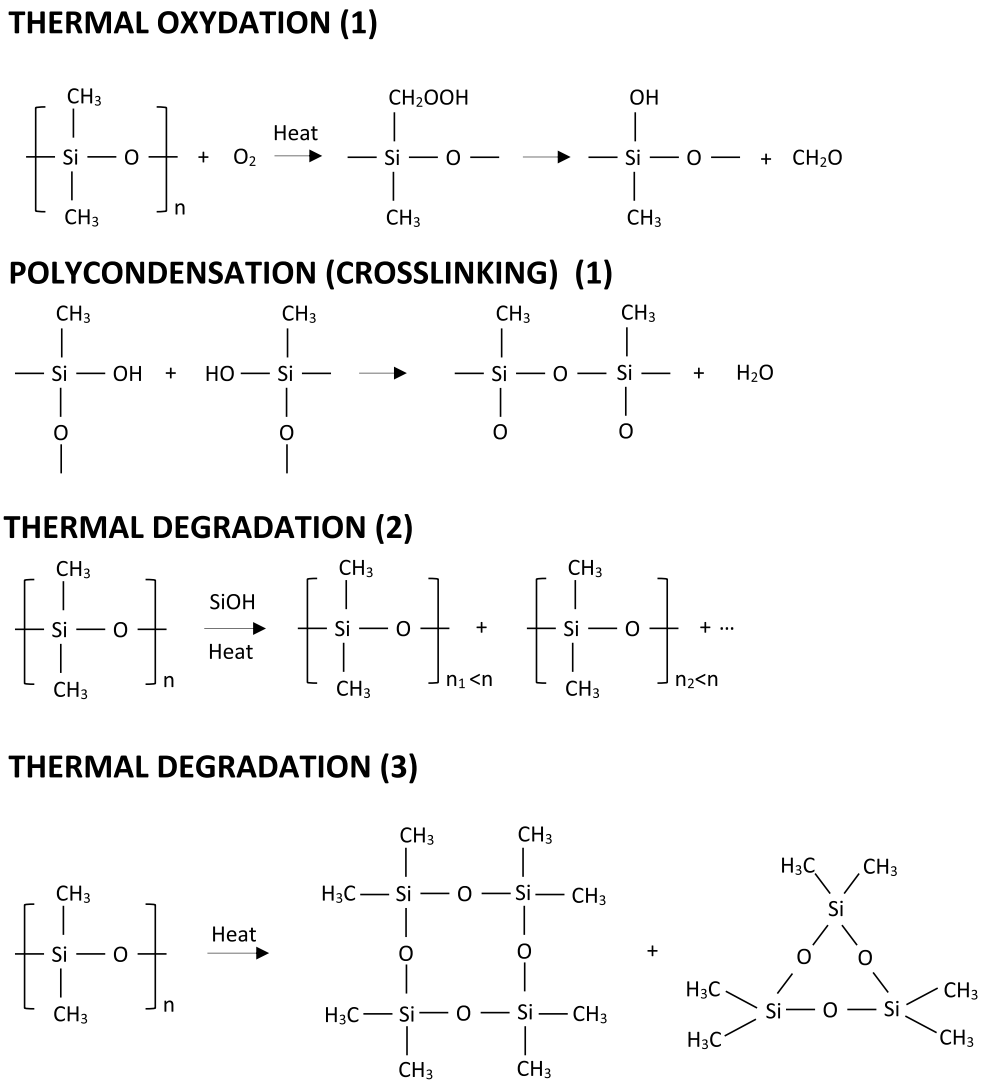

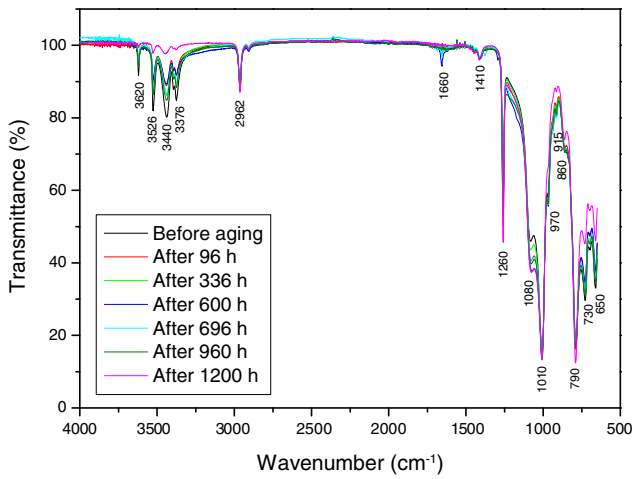

FIGURE 8 ATR-FTIR spectra of pristine and aged SiR under thermal for different aging times [Color figure can be viewed at wileyonlinelibrary.com]

the Figure 9. The contact angle of the original specimen was approximately 135°.

Independently of the aging mode, the contact angle (i.e. hydrophobicity) decreased during aging with a jump occurring at 600 h. However, the values of this angle in the case of the combination of thermal and electrical aging were lower and the difference was greater beyond 700 h. The decrease was due to the oxidation of the polymer in which some Si—CH_3 hydrophobic bonds were replaced by more hydrophilic Si—OH bonds. The jump was due to the disappearance of hydrophilic OH groups owing to the polycondensation. Indeed, the rate of the hydrophobic Si—CH_3 groups became more important than that of the hydrophilic Si—OH groups.[33] The decreasing contact angle after 700 h was related to the increase in roughness resulting from the degradation of the polymer surface and to the decrease in crystallinity.[3] The jump between 600 and 700h is linked to the breaking of Si—OH bonds under effect of heat as mentioned in the

TABLE 1 Wave numbers of main peaks or bands, their functional groups and their relative intensities (normalized to the most intense peak at 790 cm^{-1}) in the case of pristine and aged SiR

		Absorption intensity of peak (%)						
Wave-number (cm^{-1})	**Functional groups**	**P**	**96 h**	**336 h**	**600 h**	**696 h**	**960 h**	**1200 h**
3800–3200	OH	24	14	17	13.4	16.8	19.1	4
1260	$Si—CH_3$	49.9	62.3	53.9	67.7	62.3	74.6	57.4
790	$Si—(CH_3)_2$	95	94	92	92	90	90	100 (ref)
730	$Si—(CH_3)_3$	64.6	60	62.4	59.6	61.8	62.9	52.3
1080–1010	Si—O—Si	61.4	63	64.5	71.3	68	69	71.6
1615–1590	OH of water of crystallization (i.e., hydration)	0	0	0	7.8	5	0	0

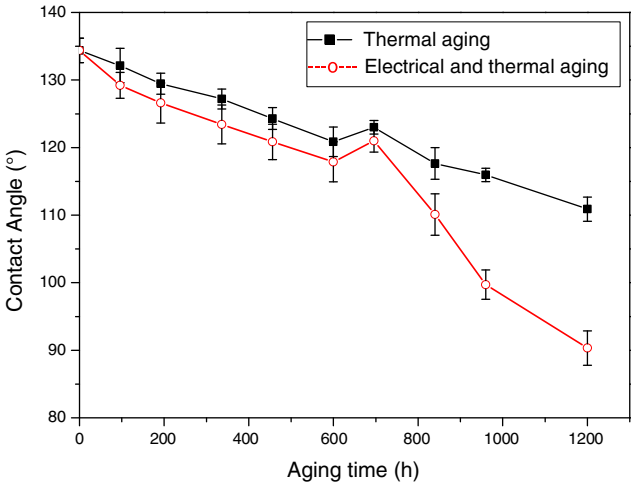

FIGURE 9 Change in contact angle versus aging time for the two used aging modes [Color figure can be viewed at wileyonlinelibrary.com]

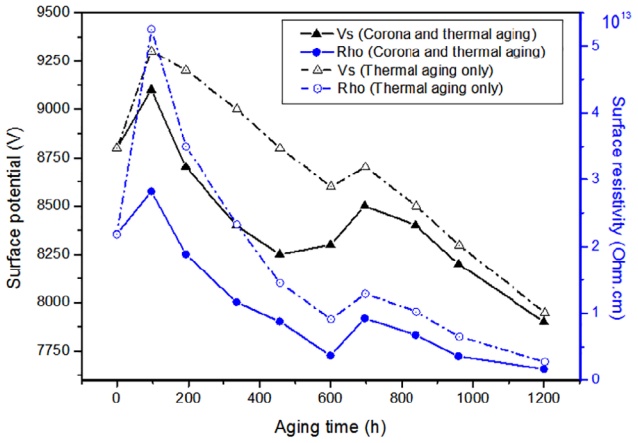

FIGURE 10 Surface potential and surface resistivity as a function of aging time [Color figure can be viewed at wileyonlinelibrary.com]

FTIR parts (Section 3.3). Indeed the disappearance of Si—OH hydrophilic groups at the beginning of reaction (2) (starting from 600 h) induces the increase of the rate of the $Si—CH_3$ hydrophobic groups.[33] The decreasing contact angle after 700 h was related to the increase in roughness resulting from the degradation of the polymer surface and to the decrease in crystallinity.[3] An in-depth study of the parameters, which govern the wettability of the surface, in particular the crystalline phases, the chemical nature, and the roughness of this surface was carried out by Mandar et al.[34] In this study, the contact angle is high for crystalline materials while it is low for amorphous ones. Indeed amorphous surfaces are usually rougher than crystalline ones.

The difference between the two aging modes was related to the roughness generated by the corona discharge.

Ultimately, there was generally a decrease in the hydrophobicity during accelerated aging. The same trend was also observed using natural aging on the polydiméthylsiloxane (silicon elastomer).[28] The decrease in hydrophobicity promoted the formation of water droplets and water channels, resulting in an electrical discharge at the surface of the insulator in use. Successive and repeated electrical discharges on the surface of the insulator can then cause a loss of electrical properties of the insulator.

3.5 | Surface potential and resistivity

The effect of aging was approached by correlating the surface potential V_s obtained under electron irradiation in vacuum of SEM and the surface resistivity ρ_s in air. Figure 10 illustrates the aging time dependence for both surface potential and surface resistivity of aged SiR. V_s evolution as a function of aging time showed that Vs started from 8.8 kV corresponding to non-aged samples. In this figure and regardless of the aging mode, the potential V_s (and ρ_s) decreased except during two small periods of aging (between 0 and 96 h and between 600 and 696 h) where it increased.

It was found also that the values of the surface potential corresponding to thermal aging alone were higher than those of combined aging modes. Moreover, for both aging types we obtain the same values for V_s and for ρ_s after 1200 h because the material, being completely degraded, has the same chemical composition and the same roughness in both cases.

Regarding the curves of surface resistivity, (Figure 10) the same behavior as surface potential was observed. Moreover, it can be seen that the surface potential and the resistivity had evolutions similar to that of the contact angle (Figure 9) except at the beginning of aging where the latter decreased. The evolution of V_s and ρ_s can be correlated with either roughness or modification of the chemical composition.

As supported by ATR-FTIR analysis, at the beginning of aging, the material loosed its moisture, leading to an increase of the surface potential (and surface resistivity). Whereas, when the aging time reached about 96 h, this trend was reversed. The decrease until 600 h of these quantities indicated that the material was subjected to a phenomenon of side chain scission and the generation of thermo-oxidation products. During this period, the phenomenon of polycondensation took place as soon as enough SiOH groups were formed.

These processes increased the density and mobility of the charge carriers leading to an increase of conductivity and hence to a decrease of V_s and ρ_s. The decrease was followed by an increase up to 696 h related to the desorption of the water formed during the polycondensation (which made the surface of the polymer less conductive). Once the water was desorbed, redundant SiOH groups contributed to the breaking of SiR molecules to give smaller molecular chains,[3] which promoted the mobility of the charge carriers and increased the conductivity of the polymer again.

In the case of the combination of thermal and electrical aging the values obtained for measured quantities (V_s and R_s) were lower than those obtained in the case of thermal aging alone. This is because of the stronger degradation of SiR that produced more defects. Moreover, the positive corona discharge modified the surface of the polymer by ionic erosion increasing its roughness. The increase of the roughness causes the increase of secondary electron emission[35] that decreases the surface potential. In addition, the implanted positive corona charge contributes to this decrease.

From a solid physics point of view, the decrease of V_s or ρ_s can be explained by considering the modification of the polymer band structure. Indeed, an increase of mobility and density of charge carriers and also an increase of density of generated defects could emphasize the disorders in the material (i.e., higher density of defects). This leads to increased numbers of localized energy levels within the normally forbidden band of the insulator.[36,37] It is then very difficult to distinguish between the bottom of the conduction band and the top of the valence band with the bandtails. Therefore, as the thermal aging time increased, the tail width of the localized states in the band gap increased leading to a decrease in band gap of aged SiR.[38] Based on these considerations, the behavior of surface potential as well as that of resistivity during aging can be interpreted. At the beginning of thermal aging, the increase of both quantities was due to the removal of moisture and the disappearance, therefore, of the energy levels of the corresponding defects in the band gap. This resulted in an increase of this band gap and then a decrease of dielectric constant of SiR. After this period, the creation of new defects decreased the band gap and increased the dielectric constant of SiR. This process allowed electrons to be promoted to the conduction band with lower energies of excitation leading to an increase of leakage current and hence a decrease of its resistivity and surface potential.

4 | CONCLUSION

In this work, the effect of accelerated thermal aging on SiR at 190°C was discussed and characterized by various techniques (FTIR, SEM, and EDS). The results showed that the electrical properties of insulation deteriorate, in particular, the surface potential and the surface resistivity. The evolutions of these two quantities during aging are perfectly correlated and lower values of V_s and ρ_s were obtained at the end of aging. This reduction has been explained based on a three-step mechanism, first oxidation, and then crosslinking of the polymer (polycondensation). The degradation of the polymer is the third and longest step. This degradation was observed using SEM images showing an increase of surface roughness with aging. These explanations are supported by the results of the FTIR analysis. This analysis showed mainly the modification of the Si—CH_3, Si—O—Si, and OH bonds in adequacy with the proposed mechanism and consequently allows the explanation of the evolution of V_s and ρ_s. The combination of both thermal and electrical effects led to a more pronounced deterioration of the polymer. The measured values of V_s and ρ_s are lower than those obtained during the single thermal aging and their evolutions during the aging time are still correlated. In this case, roughness is greater compared to thermal aging alone.

Any new insight into this problem is a step further in preventing failure of the insulation and increasing its useful lifetime.

ACKNOWLEDGMENTS

The authors would like to express their deepest gratitude to Wacker Chemie GmbH, Germany and the scientific staff of the High Voltage Laboratory of the University of Applied Sciences ofZittau/Goerlitz, Germany for supplying the samples. They also want to thank the Algerian Ministry of Higher Education and Scientific Research for supporting this work through the project PRFU A01L07UN150120180005.

ORCID

El Hadi Belhiteche https://orcid.org/0000-0002-1906-7980

REFERENCES

[1] R. Hackam, *IEEE Trans. Dielectr. Electr. Insul.* **1999**, *6*, 557.
[2] P. Mishra, R. Gautam, R. Vinu, R. Sarathi, *Polym. Eng. Sci.* **2019**, *59*, 182. https://doi.org/10.1002/pen.24887.
[3] J. Grasaesom, S. Thong-om, W. Payakcho, B. Marungsri, *World Academy of Science, Eng. Technol. Int. J. Electr. Comput. Eng.* **2011**, *5*, 1896.
[4] N. Hidayah Ismail, M. Mustapha, *Polym. Eng. Sci.* **2018**, *58*, E36. https://doi.org/10.1002/pen.24822.
[5] Y. Zhou, Y. Zhang, L. Zhang, D. Guo, X. Zhang, M. Wang, *IEEE Trans. Dielectr. Electr. Insul.* **2016**, *23*(2),748.
[6] Stanislaw M. Gubanski Outdoor Polymeric Insulators: Role of Corona in Performance of Silicone Rubber Housings, 2015 Annual Report Conference on Electrical Insulation and Dielectric Phenomena.
[7] B. Marungsri, H. Shinokubo, R. Matsuoka, *IEEE Trans. Electr. Insul.* **2006**, *13*, 129.
[8] Y. A. Bencherif, A. Mekhaldi, J. Lobry, P. Bonnaud, *J. Electr. Eng. Technol.* **2019**, *15*.
[9] C. Chen, Z. Jia, X. Wang, H. Lu, Z. Guan, *IEEE Trans. Dielectr. Electr. Insul.* **2015**, *22*(1), 313.
[10] Z. Lin, X. Guo, Z. He, X. Liang, M. Wang, G. Jin, *Polym. Eng. Sci.* **2020**. https://doi.org/10.1002/pen.25568.
[11] N. I. N. Ismail, A. Ansarifar, M. Song, *J. Appl. Polym. Sci.* **2014**, *131*(22), 41061. https://doi.org/10.1002/app.41061.
[12] S. Kashi, R. Varley, M. De Souza, S. Al-Assafi, A. Di Pietro, C. de Lavigne, B. Fox, *Polym.-Plast. Technol. Eng.* **2018**, *57*, 1687.
[13] G. F. Leal Ferreira, O. N. Oliveira Jr., J. A. Giacometti, *J. Appl. Phys.* **1986**, *59*(9), 3045.
[14] S. I. Wais, D. D. Giliyana, *Am. J. Modern Phys.* **2013**, *2*(2), 46.
[15] M. Bi, J. Yang, X. Chen, T. Jiang, A. Pan, Y. Dong, *IEEE Power Energy Soc. Section* **2020**, *8*, 128407.
[16] N. S. Kasalkova, P. Slepicka, Z. Kolska, V. Svorcik, *Wettability and Other Surface Properties of Modified Polymers*, Edit Intech Open, Tarbiat Modares University, Iran **2015**.
[17] Toshiyuki Sugimoto, Takuya Aoki Measurement of wettability for polymer materials using non-contact surface resistivity tester, Proc. 2016 Electrostatics Joint Conference.
[18] R. Saldivar-Guerreroa, R. Hernández-Corona, F. A. Lopez-Gonzalez, L. Rejon-Garcia, *Electr. Power Syst. Res.* **2014**, *117*, 202.
[19] N. Jonassen, I. Hansson, A. R. Nielsen, *Ins Phys Conf* **1979**, *48*, 215.
[20] I. Nansson, N. Jonassen, *J. Electrost.* **1978**, *4*, 335.
[21] F. Vila, G. M. Sessler, *J. Electrost.* **2001**, *51–52*, 146.
[22] B. Vallayer, G. Blaise, D. Treheux, *Rev. Sci. Instrum.* **1999**, *70*, 3102.
[23] M. Belhaj, O. Jbara, M. N. Filippov, E. I. Rau, M. V. Andrianov, *Appl. Surf. Sci.* **2001**, *177*, 58.
[24] A. Fatihou, N. Zouzou, G. Iuga, L. Dascalescu, *J. Phys.: Conf. Ser.* **2015**, *646*(1), 012035.
[25] G. Socrates, *Infrared and Raman Characteristic Group Frequencies*, John Wiley & Sons Ltd, Baffins Lane, Chichester **2001**.
[26] G. Mathew, J. M. Rhee, C. Nah, D. J. Leo, *Polym. Eng. Sci.* **2006**, *46*(10), 1455. https://doi.org/10.1002/pen.20613.
[27] H. Zhang, L. Yan, S. Zhou, H. Zou, Y. Chen, M. Liang, X. Ren, *Polym. Eng. Sci.* **2020**, 1. https://doi.org/10.1002/pen.25587.
[28] D. Ghosh, D. Khastgir, *ACS Omega* **2018**, *3*, 11317.
[29] K. Xiang, G. Huang, J. Zheng, X. Wang, G. Li, J. Huang, *J. Polym. Res.* **2012**, *19*, 9869.
[30] N. Grassie, I. G. Macfarlane, *Eur. Polym. J.* **1978**, *14*, 875.
[31] Hui Zhang, YoupingTu, Yi Lu, Zhuo Xu, Conghui Chen, Lifang Xie" Study on aging characteristics of silicone rubber insulator sheds using FTIR", IEEE International Symposium on Electrical Insulation (ISEI), 10-13 June 2012, San Juan, Puerto Rico, USA, **2012**.
[32] S. Hanada, M. Miyamoto, N. Hirai, L. Yang, Y. Ohki, *High Voltage* **2017**, *2*, 92.
[33] Y. Zhu, *Polym. Test.* **2019**, *74*, 14.
[34] M. M. Shirolkar, D. Phase, V. Sathe, J. Rodríguez-Carvajal, R. J. Choudhary, S. K. Kulkarni, *J. Appl. Phys.* **2011**, *109*, 123512.
[35] S. Rondot, O. Jbara, S. Fakhfakh, R. Belkorissat, J. M. Patat, *Nucl. Instrum. Methods Phys. Res.* **2011**, *269*, 2117.
[36] B. G. Streetman, *Solid State Electronic Devices*, 3rd ed., Prentice Hall, Englewood Cliffs, New Jersey **1995**.
[37] R. Jayakrishnan, C. SudhaKartha, K. P. Vijayakumar, S. A. Khan, D. K. Avasthi, *J. Appl. Phys.* **2008**, *103*, 023709.
[38] D. Bouguedad, O. Jbara, S. Rondot, A. Mekhaldi, A. Hadjadj, *IEEE Trans. Dielectr. Electr. Insul.* **2012**, *19*(3), 981.

How to cite this article: Belhiteche EH, Rondot S, Moudoud M, Dony P, Jbara O. Electrical insulation properties of silicone rubber under accelerated corona and thermal aging. *Polym Eng Sci*. 2020;1–10. https://doi.org/10.1002/pen.25610